Publishing Excellence Inspiring Progress
ARISTON PUBLICATIONS
MatSci Express
ISSN: 2997-8440 www.aristonpubs.com/matsci-express https://doi.org/10.69626/mse.2026.0147

RESEARCH ARTICLE

Structural and Optical Properties of $Mg_xZn_{1-x}S$ (x = 0.0 and 0.004) Nanoparticles

Ftema W. Aldbea [1,*], Salma Alsanousi Mannaa [1], Salem M. Aldosari [2], Nourah Mohammed Salih [1], Ali Adam Ali [3], Ali Basheer Yousuf [3], A. Sharma [4], Pramod K. Singh [5]

ABSTRACT: Pure and Mg-doped zinc sulfide nanoparticles ($Mg_xZn_{1-x}S$, where x = 0.0 and 0.004) were prepared using a sol–gel method, followed by calcination in air at 200 °C for 2 h. The structural, morphological, elemental, and optical characteristics of the resulting materials were examined using XRD, FE-SEM combined with EDS, and UV–visible spectroscopy. XRD analysis showed that both samples have a cubic ZnS structure; however, in the doped material, minor MgS and MgO impurity phases appeared because the calcination temperature was not high enough to achieve complete crystallization. After Mg doping, the diffraction peaks moved to higher 2θ angles, in line with the lattice parameter, confirming that Mg atoms were incorporated into the ZnS nanoparticles. Furthermore, doping led to an increase in the average crystallite size, reaching 2.72 nm, as well as in the microstrain, which arose from the impurity phases and lattice distortion. An increase in the lattice parameter (from 5.38 to 5.39 Å) and in the unit cell volume (from 155.912 to 156.320 $Å^3$) was also noted. FE-SEM analysis revealed that the pure ZnS powder was composed of agglomerated grains, while the doped sample exhibited stronger agglomeration and porosity, with visible voids. EDS analysis verified the presence of Zn and S in the pure ZnS and of Zn, S, and Mg in the doped sample. The reflectance edge was observed to shift from roughly 367 nm for pure ZnS to about 206 nm after the addition of Mg. In addition, the absorption edge shifted toward the visible region, and the optical energy gap declined from 3.6 to 1.8 eV. This narrowing of the band gap is a consequence of lattice expansion together with the presence of defects and impurity phases. Based on the calculated optical energy gap, it can be proposed that Mg-doped zinc sulfide nanoparticles may hold potential for applications in photolytic processes.

Keywords: Sol–Gel Synthesis; ZnS Nanoparticles; Magnesium Doping; Nanostructure; Optical Band Gap; Photocatalytic Potential.

Received: 21 June 2026; Revised: 01 July 2026; Accepted: 19 July 2026; Published Online: 15 August 2026

1. INTRODUCTION

Zinc sulfide has attracted tremendous attention due to its good chemical and physical properties. It is considered to be one of the promising II–VI semiconductor materials [1] mainly because of its wide band gap ranging from 3.6 to 3.8 eV, low toxicity and natural abundance [2]. It has been applied as an important material in many fields, such as solar cells, optoelectronic devices, batteries, photocatalysis, biomedical and sensors [3]. The crystal structure can be altered by thermal treatment. A cubic zinc blende structure of the F-43m space group is generally formed at a calcination temperature below 400 °C, and a hexagonal wurtzite structure with the P63mc space group is formed at a calcination temperature of more than 400 °C [4, 5]. Since the structural features significantly affect optical and electronic

[1] Physics department, Faculty of Science, Sebha University, Libya.
[2] Material Science Research Institute, King Abdulaziz City for Science and Technology (KACST), Riyadh 11442, Saudi Arabia.
[3] Department of Chemical Engineering, Faculty of Engineering, Sebha University, Libya.
[4] Metal Extraction and Recycling Division (MER), CSIR-National Metallurgical Laboratory, Jamshedpur-831007, India.
[5] Centre of Excellence in Solar Cell and Renewable Energy, Department of Physics and Environmental Sciences, Sharda School of Engineering and Science (SSES), Sharda University, Greater Noida, Uttar Pradesh, 201310, India.

* Author to whom correspondence should be addressed: fte.aldbea@sebhau.edu.ly (Ftema W. Aldbea)

© Ariston Publications 2026. All rights reserved.

properties, it is vital to precisely control the crystal phase and defect chemistry of ZnS.

The structural and optical properties of ZnS can be altered by replacing Zn with various elements, such as Fe, Cu, Ti, Sn, In, Cr, Mn, Ag, Au, Se, Li, and Mg [5–12]. Among them, Mg has been extensively studied since the incorporation of Mg into the ZnS lattice could alter the crystallinity, modify the absorbance and tune the energy gap [11, 13]. Hence, a number of studies were devoted to Mg-doped ZnS aiming to adjust the band gap for aforementioned applications. Mg/ZnS was synthesized by a hydrothermal process with different Mg concentrations (0.01–0.05). Increasing the Mg doped content reduced the lattice parameter and enhanced the diffraction peak intensities. When the Mg concentration was 0.05, the absorption onset was changed from a longer to a shorter wavelength (blue shift) and the energy gap was increased to 3.47 eV. This energy gap increase could be ascribed to the difference in ionic radius between Zn^{2+} and Mg^{2+} as well as the difference in electronegativity [14]. In another report, Mg was doped into ZnS by a sol–gel method with the concentration of 0.1, 0.2 and 0.3 M. In this case, the energy band narrows from 3.48 to 2.58 eV. The narrowing was explained by the shift of the conduction band to a lower energy due to Mg ions [15]. In contrast, an increase of about 1 eV in the energy gap was found when Mg was introduced at a concentration of 0.1 by a solvothermal route. This energy gap increase was related to the perturbation of the electronic properties caused by Mg^{2+} in ZnS structure [16]. The above different effects of Mg doping content on the optical properties of ZnS further confirm that the optical response of Mg-doped ZnS is not only controlled by the Mg content. The synthesis method, particle size, defect state, impurity phase and calcination condition also take part in the control.

The majority of the reported works focused on the wide range of Mg concentration from 0.01 to 1. Therefore, the very low doping zone has not been explored in detail. Although a very low doping content of Mg may cause the Mg to incorporate into the ZnS lattice and induce a slight alteration of the crystal structure, a minor secondary phase may be formed when the prepared conditions change. It is important to understand the initial doping stage of Mg since it may provide the influence of low content Mg on the crystallite size, micro-strain, lattice parameters, morphology, absorbance, reflectance and band gap. Besides, the low doping level plays a practical role since it might tune the properties while keeping a small disruption of the host lattice. Hence, the present work focuses on the effect of very low content of Mg on $Mg_xZn_{1-x}S$ nanoparticles with x = 0.0 and 0.004. The selection of x = 0.004 is much lower than the Mg content commonly reported in the literature. In this way, a low content of Mg can enable the observation of the incorporation of Mg and defects in Mg-doped ZnS and the impact of these factors on ZnS.

The samples were prepared by a sol–gel method and calcinated at 200 °C in air for 2 h. The low calcination temperature was selected since it is lower than the cubic-to-hexagonal transition range and is expected to be favorable for the formation of cubic ZnS. The structural, morphological, elemental and optical properties were investigated by X-ray diffraction, field emission scanning electron microscopy combined with energy dispersive X-ray spectroscopy and UV–visible spectroscopy. The XRD pattern demonstrated that both pure and doped samples had a cubic structure of ZnS, although the doped sample contained a few impurity phases of MgS and MgO. The diffraction peak positions were shifted to higher 2θ, which further confirmed the incorporation of Mg into ZnS lattice. The average crystallite size was increased from 2.48 to 2.72 nm after Mg doping, while the micro-strain was also increased due to the existence of impurity phases and lattice disturbance. The lattice parameter was slightly increased from 5.38 to 5.39 Å and the cell volume increased from 155.912 to 156.320 $Å^3$. The FE-SEM images clearly showed a agglomerated grain for pure ZnS, whereas the Mg-doped sample displayed a stronger agglomeration and porosity with some voids. The EDS confirmed an existence of Zn and S for pure sample and Zn, S and Mg for the doped sample. The reflectance onset was changed from about 367 nm (pure ZnS) to about 206 nm after Mg doping. The absorption onset was altered to the visible region, and the optical energy gap decreased from 3.6 to 1.8 eV. The decrease of the energy gap was attributed to lattice expansion, defect formation and impurity phases. The narrowed band gap suggests that the present Mg-doped ZnS might be suitable for photocatalytic application. In this paper, we report the synthesis of pure and Mg-doped ZnS nanomaterials with very low content of Mg (x = 0.004) by a sol–gel route and show the influence of such a low Mg doped content on the cubic structure, surface morphology, elemental composition and optical band gap of ZnS.

2. EXPERIMENTAL DETAILS

2.1. Synthesis of pure and Mg-doped ZnS nanoparticles

The preparation of the undoped ZnS nano-powder followed the procedure reported in our earlier work [17]. For the Mg-doped sample, zinc acetate dihydrate ($Zn(O_2CCH_3)_2{\cdot}2H_2O$, Sigma-Aldrich, 99.5% purity), thiourea (CH_4N_2S, Sigma-Aldrich, 99% purity), and magnesium nitrate hexahydrate (Alfa Aesar, 98% purity) were used as starting materials. The magnesium nitrate hexahydrate was added in an amount corresponding to a nominal Mg content of x = 0.004 in $Mg_xZn_{1-x}S$. The precursors were first dissolved separately in methanol and distilled water. These solvents were chosen to ensure complete dissolution of the metal salts and thiourea before mixing. The solutions were then combined and stirred at 50 °C for 10 min. Ammonia solution was added dropwise to the zinc/thiourea/magnesium mixture to adjust the pH to 7. The ammonia also helped to control hydrolysis and condensation during gel formation. Under continuous stirring at 50 °C, the mixture became transparent and gradually turned into a homogeneous gel. Stirring was maintained for 4 h at 50 °C to obtain a fine powder. The resulting Mg/ZnS powder was dried at room temperature for 24 h to remove

© Ariston Publications 2026. All rights reserved.

residual solvent. The dried powder was then calcined at 200 °C for 2 h in air. This relatively low calcination temperature was selected to promote crystallization while keeping the treatment below the cubic-to-hexagonal transition of ZnS. After calcination, the sample was allowed to cool naturally to room temperature before characterization. For comparison, the undoped ZnS sample was prepared by the same sol–gel route without adding the magnesium precursor. The preparation steps for the pure and Mg-doped ZnS samples are summarized in Figure 1.

2.2. Characterization techniques

The crystal structure of the samples was examined by X-ray diffraction (XRD) using a Bruker D8 Advance diffractometer with monochromatic Cu-Kα radiation (λ = 1.5406 Å). The diffraction patterns were recorded at room temperature in the 2θ range of 20° to 80°. The surface morphology and elemental composition were investigated using a field emission scanning electron microscope (Zeiss FESEM Ultra PLUS) coupled with energy dispersive X-ray spectroscopy (EDS). EDS spectra were collected from selected regions of the samples to confirm the presence of the expected elements. Optical properties were measured using a Perkin-Elmer Lambda 900 UV/vis spectrophotometer over the wavelength range of 200–900 nm. The XRD data were used to evaluate phase formation and structural parameters, while the FESEM images provided information on grain morphology and agglomeration. The UV/vis spectra were recorded to examine the reflectance and absorbance behavior of the pure and Mg-doped ZnS samples. All measurements were carried out under ambient conditions.

3. RESULTS AND DISCUSSION

3.1. X-ray diffraction analysis

The XRD patterns of $Mg_xZn_{1-x}S$ (x = 0.0 and 0.004) are shown in Figure 2 and both samples exhibited a cubic ZnS structure. However, there were additional peaks for the doped sample, which correspond to the formation of MgS (JCPDS no. 65-5548) [18] and MgO (JCPDS no. 01-045-0946) [19]. The formation of these impurity phases in the doped sample can be explained by an insufficient calcination temperature of 200 °C, which was not enough to generate phase pure Mg-doped ZnS [19]. It is well known that it is difficult to obtain a phase pure sample of Mg-doped ZnS at low temperature. The peaks of the doped sample were found to be shifted towards higher 2θ values when compared with the pure sample. This is an indication that Mg ions have been successfully incorporated into the ZnS lattice as the substitution of Zn^{2+} by Mg^{2+} causes a distortion in the crystal structure, and thus a change in the diffraction angle [19].

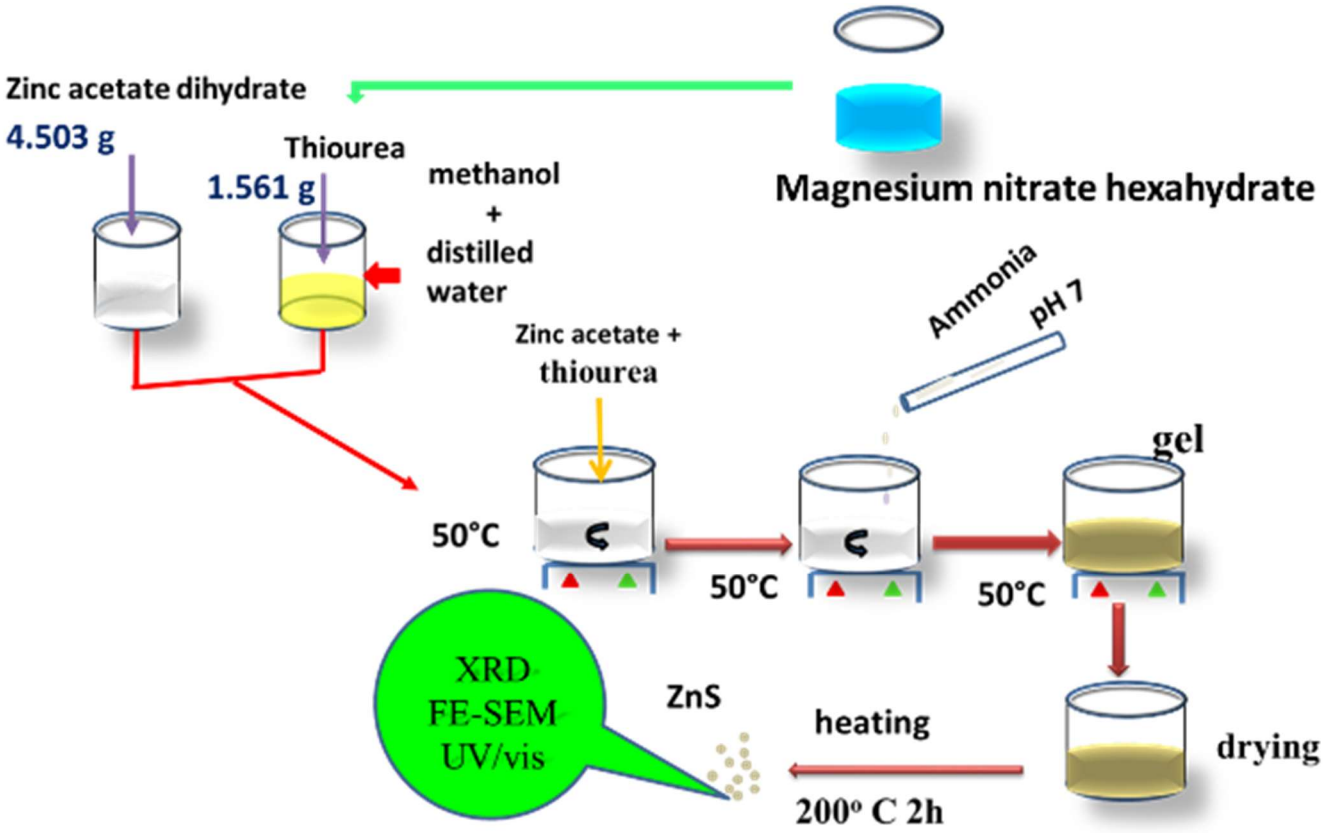


Fig.1. The preparation steps of pure and doped ZnS samples.

© Ariston Publications 2026. All rights reserved.

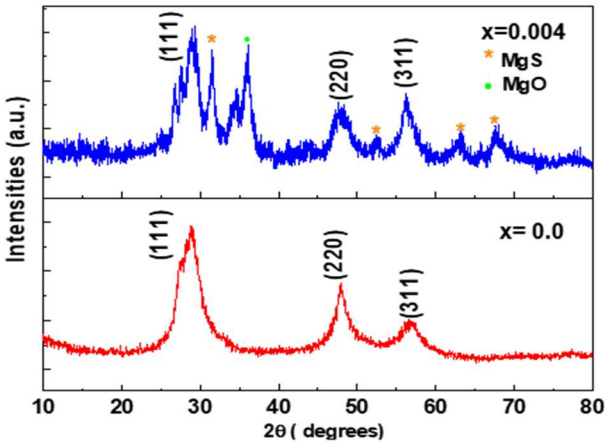


Fig. 2. XRD patterns of $Mg_xZn_{1-x}S$ (x = 0.0 and 0.004) calcined at 200 °C for 2 h.

The crystallite size (D) of the pure and doped samples was calculated using the Scherrer equation [20]:

$$D = \frac{K\lambda}{\beta cos\theta} \quad (1)$$

Where D is the crystallite size, K is the shape factor (K = 0.9), θ is the diffraction angle, λ is the wavelength of the X-ray radiation (1.54056 Å), and β is the full width at half maximum (FWHM) of each diffraction peak. The average crystallite size values are shown in Table 1. The crystallite size was increased from 2.48 nm for the pure sample to 2.72 nm for the doped sample. This increase suggests that the addition of Mg ions to the ZnS samples promotes the crystallite growth, possibly due to the decrease in the density of nucleation sites [15]. However, the increase in the crystallite size has resulted in an increase in the micro-strain (ε), as also shown in Table 1. Normally, a decrease in crystallite size would cause an increase in micro-strain, the opposite effect observed as a result of the impurity phases formed in the doped sample.

Table 1. Crystallite size, micro-strain, lattice parameter, and cell volume values for pure and doped ZnS.

Mg concentration (x)	D (nm)	ε $x10^{-3}$	*a* (Å)	Volume V(Å^3)
0.0	2.48	6.4	5.38	155.912
0.004	2.72	7.3	5.39	156.320

The lattice parameter of the pure and doped samples was calculated using the following formula [16]:

$$a = \sqrt{\frac{\lambda^2}{4sin^2\theta}(h^2 + k^2 + l^2)} \quad (2)$$

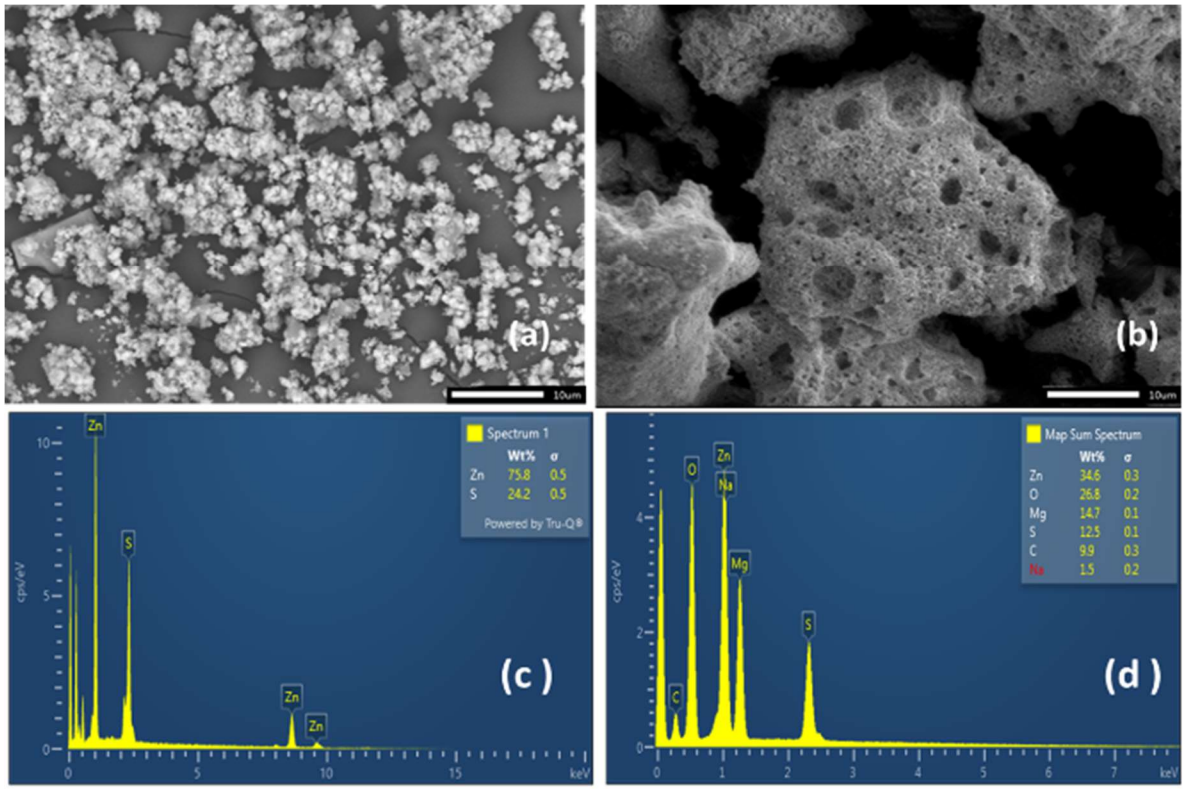


Fig. 3. FE-SEM images of (a) pure ZnS and (b) Mg-doped ZnS. EDS spectra of (c) pure ZnS and (d) Mg-doped ZnS.

© Ariston Publications 2026. All rights reserved.

Where λ is the wavelength of the Cu-Kα radiation (λ = 1.5406 Å), θ is the diffraction angle and (h, k, l) are the Miller indices. The lattice parameter values calculated are presented in Table 1. The lattice parameter was found to increase slightly from 5.38 to 5.39 Å, and these values are close to the lattice parameter of bulk ZnS (5.403 Å) [21]. The slight increase in the lattice parameter upon doping could be due to the difference in the ionic radius of Zn^{2+} and Mg^{2+} or due to the presence of impurity phases. The cell volume was also found to increase from 155.912 $Å^3$ for the pure sample to 156.320 $Å^3$ for the doped sample.

3.2. Field emission scanning electron microscopy analysis

The FE-SEM images of pure and doped ZnS samples are shown in Figure 3. The surface morphology of the pure ZnS sample (Figure 3(a)) consisted of agglomerated grains with an average size of around 2 ± 1 nm. The grains were found to be loosely packed with some interparticle spaces. In contrast, the micrograph of the doped sample (Figure 3(b)) revealed highly agglomerated grains with visible voids. The average grain size of the doped sample was calculated to be about 6 ± 1 nm. The increase in grain size upon addition of Mg ions is an indication of the increase in the crystallite size, as found from the XRD results. The greater agglomeration and porosity of the doped sample are probably due to the impurity phases formed in the sample.

The elemental composition of the samples was investigated using EDS and the results are shown in Figure 3(c) for pure ZnS and Figure 3(d) for the doped sample. The EDS spectrum of pure ZnS confirms the presence of Zn and S as the major elements. For the doped sample, the spectrum confirms the presence of Zn, S, and Mg. The detection of Mg in the doped sample proves that magnesium has been successfully incorporated into the material. The oxygen and sodium peaks in the EDS spectra originated from the starting materials and residual species.

3.3. Optical properties

The reflectance spectra of pure and doped ZnS are shown in Figure 4. The pure ZnS sample has a reflectance edge at around 367 nm; a value that is characteristic of nanocrystalline ZnS (Figure 4 (a)). Upon incorporation of Mg ions, the reflectance edge shifts significantly towards shorter wavelength and is found at around 206 nm for the doped sample (Figure 4 (b)). The significant blue shift in the reflectance edge can be attributed to lattice distortion and defect formation due to the addition of Mg ions [22]. The impurity phases such as MgS and MgO may also contribute to a change in the reflectance of the samples.

The absorbance spectra of pure and doped ZnS samples are shown in Figure 5. The pure ZnS sample (x = 0.0) displayed a sharp absorption edge in the UV range, located between 250 and 320 nm. In contrast, the doped sample (x = 0.004) shows a significant shift of the absorption edge towards the visible region, where the edge appears between 380 and 450 nm. The shift of the absorption edge towards the longer wavelength side indicates a decrease in the optical band gap. The change in the absorption edge is due the incorporation of Mg ions into the ZnS structure, which results in the formation of defect states between the valence and conduction bands. The defect states give rise to the electronic transitions at lower energy, and hence a change in the band gap. The broadening of the absorption edge of the doped sample indicates a change in the band gap and also an increase in the structural disorder, which is supported by the results obtained.

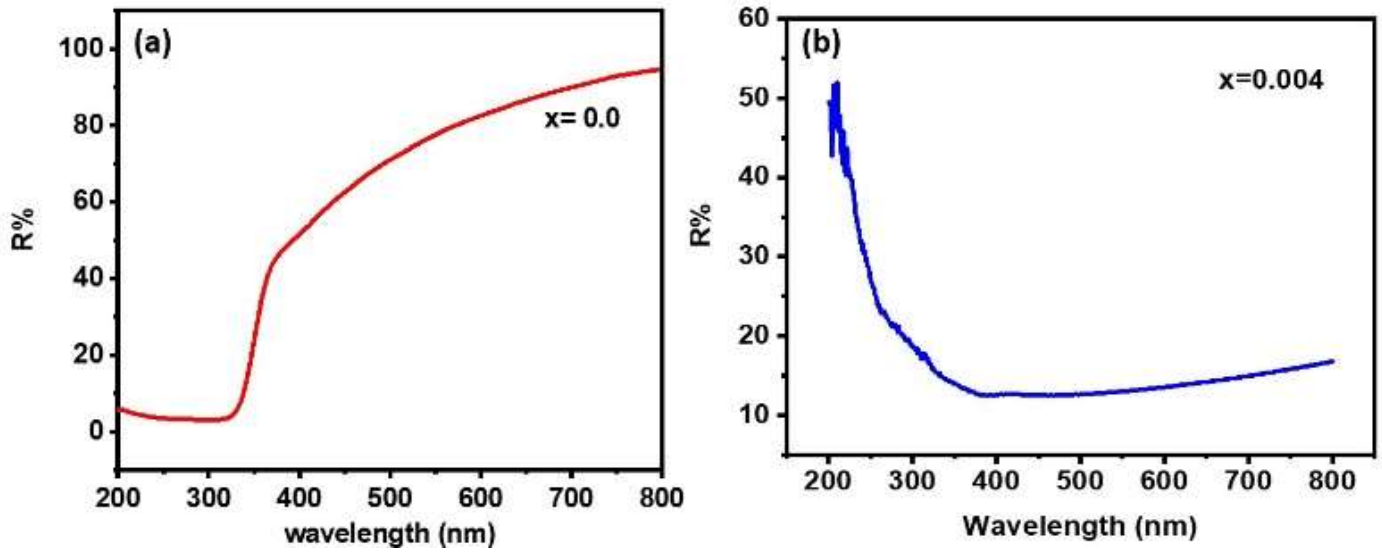


Fig. 4. Reflectance spectra of (a) pure ZnS, and (b) Mg-doped ZnS.

© Ariston Publications 2026. All rights reserved.

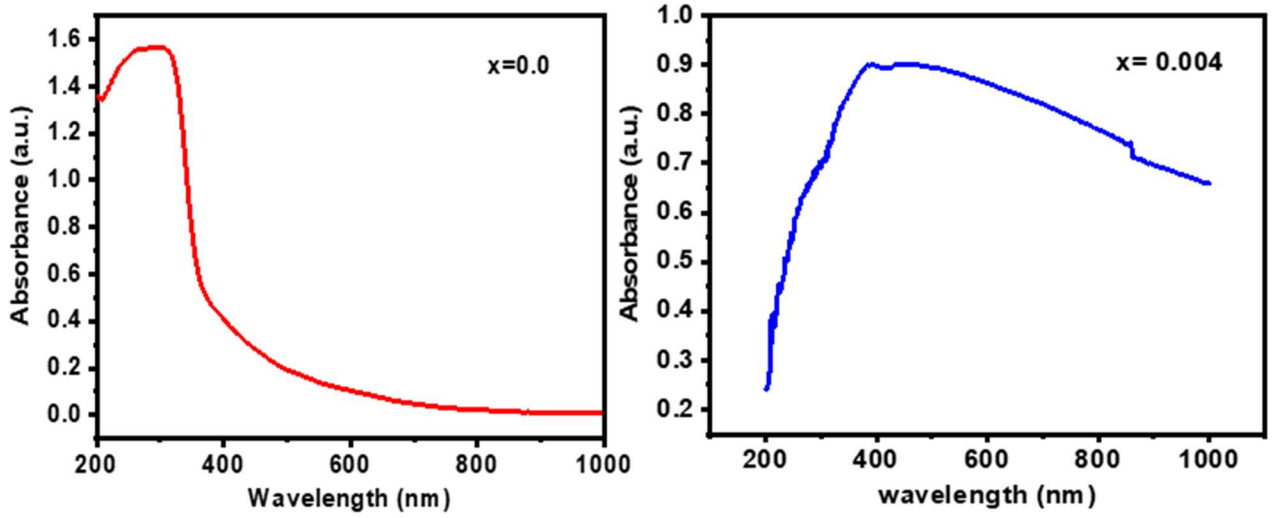


Fig. 5. Absorbance spectra of pure ZnS and Mg-doped ZnS.

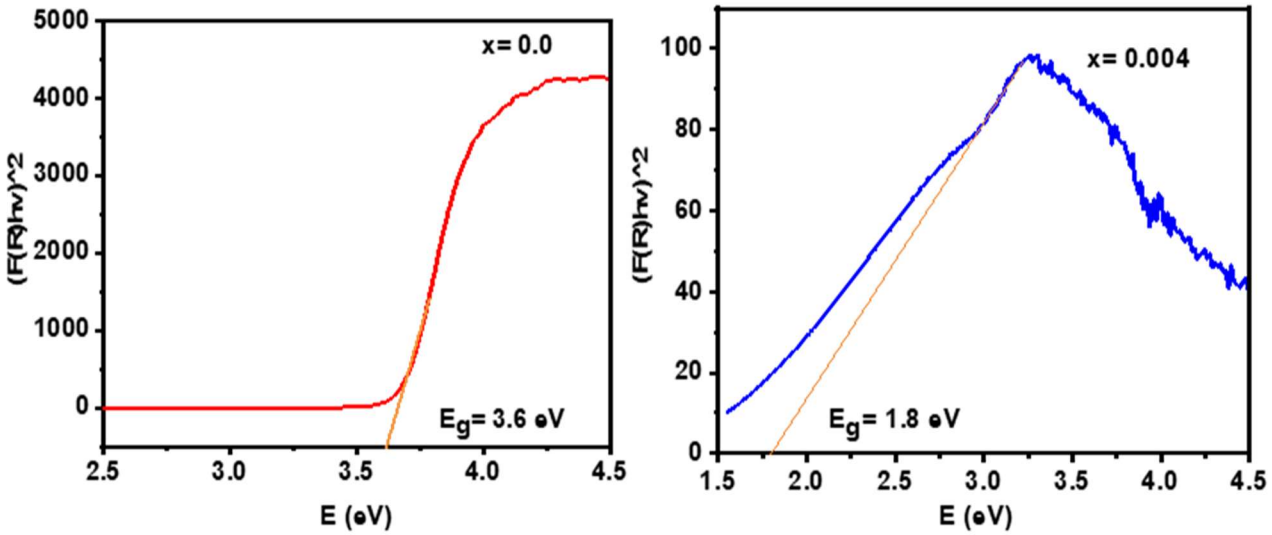


Fig. 6. Tauc plots and energy gap values of pure ZnS and Mg-doped ZnS.

The optical energy gap (Eg) values of the pure and doped samples were estimated from Tauc plots, where the Kubelka–Munk function $(F(R)\ h\upsilon)^2$ is plotted against photon energy ($h\upsilon$), where h is Planck's constant and υ is the frequency. The band gap was found by extrapolating the linear part of each curve to zero absorption. Figure 6 shows the Tauc plots of the pure and doped ZnS samples. Pure ZnS sample has an energy gap of around 3.6 eV, which is close to the band gap of bulk ZnS (3.6-3.9 eV) [24]. For the doped sample (x = 0.004), the energy gap value decreased to around 1.8 eV. The reduction in the energy gap can be due to several reasons. Firstly, the lattice expansion that was observed from the XRD results could have changed the band structure by causing a change in the overlapping of the atomic orbitals. The formation of defect states, as indicated by the absorbance results, could also have reduced the band gap by allowing electronic transitions at lower energies. The impurity phases formed in the sample could also have narrow the band gap by creating additional electronic states. The change in the band gap value from 3.6 to 1.8 eV is quite remarkable and suggests that the changes in the structural properties have had a great impact on the optical properties of the samples.

The reduction in the band gap is significant and it opens up a lot more possibilities for the application of ZnS doped with magnesium. A band gap of 1.8 eV means that the light in the visible region of the electromagnetic spectrum is absorbed by the doped sample; in other words, the amount of light absorbed in the visible region has significantly increased. This property is very desirable for photocatalysis, where a large fraction of the incident solar radiation must be absorbed for effective charge transfer processes. The combination of the enhanced visible-light absorption and the

 © Ariston Publications 2026. All rights reserved.

porous shape of the sample, which gives a large surface area for catalytic reactions to occur, means that the present ZnS doped with Mg could potentially be used as a photocatalyst for the degradation of organic pollutants.

4. CONCLUSION

ZnS nanoparticles, both pure and Mg-doped with x = 0.0 and 0.004, were prepared through a sol-gel method and calcined at 200 °C for 2 h. The XRD patterns revealed that both samples crystallized in the cubic ZnS structure. For the doped sample, small amounts of MgS and MgO phases appeared, indicating that the calcination temperature was too low to achieve a phase pure sample. Even so, the diffraction peaks shifted toward higher 2θ values, and together with a slight rise in lattice parameter and cell volume, this demonstrated that Mg had been incorporated into the ZnS lattice. After doping, the average crystallite size grew from 2.48 to 2.72 nm, while micro-0strain increased because of the impurity phases and lattice disorder. FE-SEM images revealed agglomerated grains in the pure sample, whereas the doped sample displayed a more agglomerated and porous morphology. EDS verified the presence of Zn and S in the pure sample, and of Zn, S, and Mg in the doped sample. Optical measurements indicated a marked change in the optical properties following Mg doping. The reflectance edge shifted from ~367 to 206 nm, while the absorption edge moved into the visible region. The optical energy gap dropped from 3.6 eV for pure ZnS to 1.8 eV for the doped sample, which may be linked to lattice expansion, defect states, and impurity phases. The narrowing of the band gap, along with the porous morphology, indicates that the Mg-doped ZnS nanoparticles described here could be suitable for photocatalytic applications under visible light. Future work should focus on optimizing the experimental conditions so as to obtain a phase pure sample and minimize the impurity phases.

DECLARATIONS

Conflicts of Interest

The authors declare that there is no conflict of interests.

Author's contribution statement

All authors contributed to the study's conception and design. Material preparation, data collection, and analysis were performed by all authors. The first draft of the manuscript was written by Ftema W. Aldbea, and all authors commented on previous versions of manuscripts. All authors read and approved the final manuscript.

REFERENCES

[1] Chaliha, C., Nath, B.K., Verma, P.K. and Kalita, E., **2019**. Synthesis of functionalized Cu: ZnS nanosystems and its antibacterial potential. *Arabian Journal of Chemistry*, *12*(4), pp.515-524. https://doi.org/10.1016/j.arabjc.2016.05.002

[2] Sarangi, B., Mishra, S.P. and Behera, N., **2022**. Advances in green synthesis of ZnS nanoparticles: an overview. *Materials Science in Semiconductor Processing*, *147*, p.106723. https://doi.org/10.1016/j.mssp.2022.106723

[3] Chakrabarti, A. and Alessandri, E., **2024**. Syntheses, properties, and applications of ZnS-based nanomaterials. *Applied Nano*, *5*(3), pp.116-142. https://doi.org/10.3390/applnano5030010

[4] Ma, C., Moore, D., Ding, Y., Li, J. and Wang, Z.L., **2004**. Nanobelt and nanosaw structures of II-VI semiconductors. *International journal of nanotechnology*, *1*(4), pp.431-451. https://doi.org/10.1504/IJNT.2004.005978

[5] Huang, Y.H., Jie, W.Q., Zhou, Y. and Zha, G.Q., **2013**. Structural stability, band structure and magnetic properties of ZnS and $Zn_{0.75}Cr_{0.25}S$ under pressure. *Journal of alloys and compounds*, *549*, pp.184-189. https://doi.org/10.1016/j.jallcom.2012.09.031

[6] Shakoor, I., Jabeen, U., Ahmad, I., Riaz, S., Tayyab, M., Syed, A., Bahkali, A.H., Riaz, M., Zairov, R.R. and Zafar, M.N., **2024**. ZnS and Fe-doped ZnS photocatalysts for improved visible light driven photocatalytic degradation of methylene blue. *Inorganica Chimica Acta*, *560*, p.121837. https://doi.org/10.1016/j.ica.2023.121837

[7] Ummartyotin, S., Bunnak, N., Juntaro, J., Sain, M. and Manuspiya, H., **2012**. Synthesis and luminescence properties of ZnS and metal (Mn, Cu)-doped-ZnS ceramic powder. *Solid State Sciences*, *14*(3), pp.299-304. https://doi.org/10.1016/j.solidstatesciences.2011.12.005

[8] Kumari, P., Chattopadhyay, S. and Samanta, S., **2025**. A comprehensive review on rare earth metal doped ZnS nanoparticles: structure, synthesis, properties, and applications in the realm of nanotechnology. *Discover Applied Sciences*, *7*(9), p.1011. https://doi.org/10.1007/s42452-025-07672-0

[9] Abdullah, H., Hsu, S.H., Susanto, J.B., Lin, T.J. and Kuo, D.H., **2026**. Highly Selective Photo-Valorization of Furfural-to-Furfuryl Alcohol Conversion over Oxygen Vacancy-Defected ZnS_xO1-x: $Li/Zn(OH)_2$

© Ariston Publications 2026. All rights reserved.

Nanocomposite. *Materials Today Nano*, p.100800. https://doi.org/10.1016/j.mtnano.2026.100800

[10] Shaji, N., Koshy, M.M., Balachandran, M., Deepthi, V. and Joby, A., **2026**. Synergistic engineering of Ag-Doped ZnS/SnSe heterostructures for enhanced Visible-Light photocatalytic degradation with sustainable agricultural water reuse. *Chemical Engineering Science*, p.124677. https://doi.org/10.1016/j.ces.2026.124677

[11] Choubey, S.K., Jyoti, T. and Tiwary, K.P., **2026**. Photodegradation of Methyl Orange Dye Using Mg Modified ZnS in Presence of Visible Light. *Applied Mechanics and Materials*, *933*, pp.41-49. https://doi.org/10.4028/p-MI5zNY

[12] Murugadoss, G., Venkatesh, N., Venkatesan, R., Kim, S.C., Gnanasekaran, L. and Moovendhan, M., **2026**. Synergistic enhancement of the photocatalytic and antibacterial activities of cerium and tin-doped zinc sulfide nanoparticles. *Surfaces and Interfaces*, p.108798. https://doi.org/10.1016/j.surfin.2026.108798

[13] BALNAN, İ., **2026**. Banana peel–assisted synthesis of ZnS and 5 mol% Mg-doped ZnS for photocatalytic degradation of Congo Red. *MAS Journal of Applied Sciences*, *11*(1), pp.68-80. https://doi.org/10.5281/zenodo.18920789

[14] Reddy, D.A., Kim, D.H., Rhee, S.J., Lee, B.W. and Liu, C., **2014**. Tunable blue-green-emitting wurtzite ZnS: Mg nanosheet-assembled hierarchical spheres for near-UV white LEDs. *Nanoscale research letters*, *9*(1), p.20. https://doi.org/10.1186/1556-276X-9-20

[15] Shahid, M.Y., Asghar, M., Arbi, H.M., Zafar, M. and Ilyas, S.Z., **2016**. Role of magnesium in ZnS structure: Experimental and theoretical investigation. *AIP Advances*, *6*(2). https://doi.org/10.1063/1.4942512

[16] Salima, M., Youcef, M., Bouarroudj, T., Chetoui, A., Belkhettab, I., Bezzi, H., Aoudjit, L., Zioui, D., Ziouche, A. and eddine Mekki, D., **2023**. Sunlight-assisted photocatalytic degradation of tartrazine in the presence of Mg doped ZnS nanocatalysts. *Solid State Sciences*, *143*, p.107260. https://doi.org/10.1016/j.solidstatesciences.2023.107260

[17] Waniss Aldbea, F., Abdoorhman, Z., Almahdi, R.A., Kraini, M. and Imrigha, N.A., **2023**. Structural Properties and Antibacterial Activity of Zinc Sulfide Nanoparticles. *NanoWorld J*, *9*(4), pp.127-132. https://doi.org/10.17756/nwj.2023-124

[18] Goo, N.H. and Hirscher, M., **2005**. Synthesis of the nanocrystalline MgS and its interaction with hydrogen. *Journal of alloys and compounds*, *404*, pp.503-506. https://doi.org/10.1016/j.jallcom.2004.12.192

[19] Todan, L., Predoană, L., Petcu, G., Preda, S., Culiță, D.C., Băran, A., Trușcă, R.D., Surdu, V.A., Vasile, B.Ș. and Ianculescu, A.C., **2023**. Comparative study of MgO Nanopowders prepared by different chemical methods. *Gels*, *9*(8), p.624. https://www.mdpi.com/2310-2861/9/8/624#

[20] Aldbea, F.W., Vázquez Vázquez, C., Othman, U.A., Sharma, A., Boukhachemd, A., Mailoude, O.M., Kraini, M. and Singh, P.K., **2024**. Structural and optical properties of Iodine doped zinc oxide nanoparticles. *Journal of Materials Science: Materials in Electronics*, *35*(7), p.459. https://doi.org/10.1007/s10854-024-12170-x

[21] Asfia, M.B. and Rashid, M.A., **2022**. First principles calculations of structural, electronic and optical properties of Sn-doped ZnS. *Physica B: Condensed Matter*, *646*, p.414335. https://doi.org/10.1016/j.physb.2022.414335

[22] Prabu, J.H. and Johnson, I., **2015**. Greener cum chemical synthesis and characterization of Mg doped ZnS nanoparticles and their engineering band gap performance. *Journal of Engineering Research and Application*, *5*(8), pp.99-105.

[23] O'Hara, A., Schrimpf, R.D., Fleetwood, D.M. and Pantelides, S.T., **2024**. Defect dynamics in the presence of excess energetic carriers and high electric fields in wide-gap semiconductors. *Journal of Applied Physics*, *135*(19). https://doi.org/10.1063/5.0203047

[24] Chellammal, S. and Sankar, S., **2010**. Energy gap studies of ZnS nanocrystallites. *Materials Science in semiconductor processing*, *13*(3), pp.214-216. https://doi.org/10.1016/j.mssp.2010.10.003

[25] Badar, N., Kamarulzaman, N., Chayed, N.F., Elong, K. and Yahaya Subban, R.H., **2020**, May. Band Gap Narrowıng of $Mg1\text{-}xCu_xO$ Nanostructured Materials. In *Journal of Physics: Conference Series* (Vol. 1535, No. 1, p. 012023). IOP Publishing. https://doi.org/10.1088/1742-6596/1535/1/012023

 © Ariston Publications 2026. All rights reserved.